IEEE Open Journal of
Power Electronics

Received 28 April 2025; revised 15 July 2025; accepted 27 July 2025. Date of publication 30 July 2025;
date of current version 8 August 2025. The review of this article was arranged by Associate Editor Telles Brunelli Lazzarin.

*Digital Object Identifier 10.1109/OJPEL.2025.3594307*

# Virtual-Vector-Based Predictive Torque Control for Six-Phase IM With Reduced Computational Burden and Copper Losses

**OSVALDO GONZALEZ [1], JESÚS DOVAL-GANDOY [2] (Member, IEEE), MAGNO AYALA [1] (Member, IEEE), JORGE RODAS [1] (Senior Member, IEEE), PAOLA MAIDANA [1], CHRISTIAN MEDINA [1], CARLOS ROMERO [1], LARIZZA DELORME [1] (Member, IEEE), RAUL GREGOR [1] (Member, IEEE), AND RICARDO MACIEL [1]**

[1]Department of Electronics and Mechatronics Engineering, Facultad de Ingeniería, Universidad Nacional de Asunción, Luque 110948, Paraguay
[2]Applied Power Electronics Technology Research Group, CINTECX, Universidad de Vigo, 36310 Vigo, Spain

CORRESPONDING AUTHOR: OSVALDO GONZALEZ (e-mail: ogonzalez@ing.una.py)

This work was supported in part by Facultad de Ingeniería, Universidad Nacional de Asunción, Paraguay, in part by Consejo Nacional de Ciencia y Tecnología (CONACYT)–Paraguay through "Programa de Incentivos para la Formación de Investigadores en Posgrados Nacionales (BCAS02)" for the "Programa de Doctorado en Ingeniería Electrónica" under Project PINV01-272 and Project INIC01-35, in part by SISNI Program, in part by the Government of Galicia under Grant GPC-ED431B 2023/12, in part by Spanish State Research Agency (AEI) under Project PID2022-136908OBI00/MCIN/AEI/10.13039/501100011033/ FEDER-UE, and in part by Thematic Network RIBIERSE-CYTED under Grant 723RT0150.

**ABSTRACT** Finite-control-set model predictive control (FCS-MPC) has become widely accepted in multiphase drives due to its adaptability and robust dynamic response. However, multiphase machines, characterized by low secondary plane $(x-y)$ impedance, which is absent in their three-phase counterparts, often exhibit poor current quality under conventional FCS-MPC strategies. This paper proposes a novel predictive torque control (PTC) scheme based on virtual vectors to improve $(x-y)$ current regulation by ensuring zero average $(x-y)$ voltage generation. The proposed method is compared with classic PTC, which cannot achieve proper $(x-y)$ current regulation because it uses a single switching state during the sampling period. Experimental validation includes a detailed comparison of torque and flux behavior, $(x-y)$ current mean square error, and total harmonic distortion of the fundamental stator currents, demonstrating the effectiveness of the proposed control approach under various operating conditions. Experimental results confirm reductions of approximately 79.7% in computational burden and 98.4% in copper losses when using PTC-VV compared to classic PTC. An asymmetrical six-phase induction machine is used as the case study.

**INDEX TERMS** Multiphase drives, model-based predictive control, predictive torque control, six-phase induction machine, virtual vectors.

## I. INTRODUCTION

Recently, there has been a growing interest in the use of multiphase machines characterized by a number of phases greater than three. Compared to their three-phase counterparts, these machines offer notable advantages, including improved phase current redistribution and enhanced torque production. Notably, multiphase machines can operate effectively even in the presence of faults [1].

Driven by the pursuit of more efficient and reliable solutions in power electronics, multiphase machines are increasingly adopted in high-demand electric drive applications. Their reduced torque ripple and higher power density make them ideal for use in electric ship propulsion, electric vehicles, and renewable energy systems [2]. Thus, the adoption of multiphase systems in place of the conventional three-phase can be found in some commercial examples, including six-phase and nine-phase electric trucks by Dana [3]. Audi Sport has also incorporated a six-phase drive system for the e-tron FE07 model in Formula E [4]. Also, BMW has integrated a six-phase machine with a double inverter in its iX M60 electric SUV model [5]. The incorporation of multiphase machines in the mentioned industrial applications can be attributed to their distinctive features, as described in [6].

At this point, it is essential to mention that to make efficient use of existing technology for three-phase systems, most multiphase machines used in industrial applications incorporate multiple sets of three-phase windings, with the six-phase machine being the most straightforward configuration [7].

A typical asymmetrical six-phase induction machine (IM) consists of two sets of three-phase stator windings, spatially shifted by 30°, each with its own isolated neutral point. This configuration defines two orthogonal planes based on vector space decomposition (VSD): the torque-producing $(\alpha - \beta)$ plane and the auxiliary $(x - y)$ plane [8]. This topology helps to reduce torque harmonics and suppress zero-sequence currents. Although the $(x - y)$ components do not participate in energy conversion, low-order harmonics in this plane can degrade system performance and increase copper losses.

The initial control strategies proposed for six-phase IMs, such as field-oriented control (FOC) and direct torque control (DTC), were extensions of those developed for three-phase IMs [9]. In FOC, pulse width modulation (PWM) is employed to regulate flux and torque through proportional-integral (PI) controllers, allowing simultaneous control of primary and secondary currents [10]. Meanwhile, DTC directly manages flux and torque using hysteresis controllers and a predefined switching table, although it often faces challenges like deviations exceeding hysteresis bounds [11], [12], [13].

Recently, finite-control-set model predictive control (FCS-MPC) has gained popularity in high-performance IM drives due to its effectiveness in managing multivariable scenarios [14], [15], [16]. Its advantages over classical control strategies include enhanced dynamic performance, flexibility in defining control objectives, and the incorporation of constraints [17], [18].

This method uses a discrete system model to predict future behavior based on a finite set of converter states [19]. A cost function defines control objectives, and the optimal action minimizes the function, though this can increase $(x - y)$ currents in multiphase drives. To address this, weighting factors can regulate $(x - y)$ currents [20]. However, using a single switching state limits voltage contributions in both $(\alpha - \beta)$ and $(x - y)$ planes, which affects system dynamics.

Several variations of FCS-MPC strategies for multiphase IM drives have been reported as potential solutions for regulating $(x - y)$ currents. A modulation strategy known as virtual vectors was proposed as a solution for a five-phase IM in [21] to minimize the $(x - y)$ currents. This strategy combines two active voltage vectors to be employed within a sampling period. Additionally, this strategy has been proposed for six-phase IM drives as a PCC to regulate the generation of $(x - y)$ currents [22], [23].

When FCS-MPC is utilized in motor drives specifically for torque control purposes, it is commonly known as PTC, widely regarded as an effective alternative to traditional DTC [24]. Unlike traditional table-based DTC, PTC uses online optimization rather than heuristic switching tables. It defines a cost function based on errors in torque, flux, and $(x - y)$ currents for multiphase drives, selecting the voltage vector that minimizes the cost function as the optimal selection. Therefore, PTC achieves a more precise and efficient selection of voltage vectors compared to traditional DTC [25], [26]. In addition to DTC, PTC has been evaluated alongside FOC, another widely used and well-established strategy for achieving high-performance torque control. Research studies demonstrate that PTC achieves steady-state performance similar to FOC, with slightly larger current harmonics, while offering a faster dynamic response, as discussed in [27], [28]. Furthermore, PTC presents a straightforward approach to incorporating diverse nonlinear constraints and implementing multi-variable control. As a result, PTC provides increased flexibility and emerges as a promising alternative to FOC.

PTC strategy directly regulates the flux and torque of the machine using the stator current and rotor flux components as state variables [7]. However, applying the PTC strategy in multiphase IM drives must consider the appearance of $(x - y)$ currents. In [29], speed control of a six-phase IM fed by a matrix converter was proposed using an inner PTC to mitigate the computational burden by reducing the number of valid voltage vectors. Nevertheless, it does not consider the regulation of $(x - y)$ currents. Also, a speed sensorless PTC for a five-phase IM, implemented in a three-level neutral-point clamped topology, was presented in [30]. This approach utilized a synthetic voltage vector to reduce the $(x - y)$ currents. However, the PTC strategy employed a hysteresis comparator.

A simplified PTC has also been studied for dual three-phase permanent magnet synchronous machines (PMSMs). This strategy has demonstrated methods to reduce computational burden and current harmonics [31]. However, these approaches often fail to address the challenges posed by the $(x - y)$ current regulation in six-phase IMs, where the low impedance of the secondary plane exacerbates harmonic distortions. Another PTC strategy has been applied to the PMSM, as discussed in [32]. A study aiming to reduce computational burden and current harmonics presents a simplified version of PTC for a six-phase PMSM. However, this simplified version results in a large torque ripple because only one vector is applied during the sampling period. In [33], a double-virtual-vector-based model PTC for dual three-phase PMSM was proposed to address the appearance of $(x–y)$ currents; however, it does not quantify the losses related to that plane. Recently, a sequential model PTC (SMPTC) for six-phase machines without weighting factors was presented in [34] to eliminate the weighting factor. However, it still presents some limitations in reducing the $(x - y)$ currents. Despite this, it is necessary to note that PTC is still a better strategy than PCC when it comes to reducing torque ripple, as stated in a previous study [32].

This paper builds upon the preliminary work presented in [35], where the strategy using a virtual vector based on simulation results was introduced. The aim is to regulate current harmonics in the secondary plane better while reducing torque ripple, computational burden, and copper losses in torque control. To highlight the performance of the improved PTC strategy, a comparative analysis is provided between classic PTC and PTC using virtual vectors (PTC-VV) applied to an electric drive based on an asymmetrical six-phase IM fed by a two-level VSI.

Until now, PCC has mainly used virtual vectors to mitigate effects within the $(x-y)$ plane. However, this paper proposes extending the use of virtual vectors to PTC to regulate current harmonics in the secondary plane while simultaneously reducing the computational burden and copper losses during torque regulation. Therefore, the main contributions of the proposed method can be summarized as follows.

- When comparing the proposed PTC-VV method with the classic PTC under steady-state conditions, there is an 87% reduction in the Mean Squared Error (MSE) of the $(x-y)$ currents, a 27% reduction in the total harmonic distortion (THD) of the torque, a 28% reduction in the MSE of the fundamental $(\alpha-\beta)$ currents, and a 98.4% reduction in copper losses.
- The computational burden is reduced as only 13 virtual vectors settings need evaluation, compared to the 49 voltage vectors required for the classic PTC.
- The combination of active voltage vectors, including medium-large and large vectors within the candidate group of the $(\alpha-\beta)$ plane, is assigned to opposite directions within the $(x-y)$ plane. This facilitates effective minimization of the $(x-y)$ currents for the PTC-VV.
- The proposed PTC-VV reduces the tuning process of the weighting factor in the cost function since, unlike classic PTC, it does not require the inclusion of the term related to the $(x-y)$ plane.

The paper is structured as follows: the next section provides a mathematical analysis of the six-phase IM drive, which is the primary focus of the investigated multiphase system. Section III explains the basic principles of the PTC for six-phase IM drives. Furthermore, Section IV presents experimental results for both classic PTC and PTC-VV. Lastly, the study's conclusions are summarized in the final section.

## II. MATHEMATICAL MODEL FOR SIX-PHASE INDUCTION MACHINE AND TWO-LEVEL CONVERTER

Before implementing the PTC strategy, it is crucial to consider the mathematical model of the system. This model encompasses distributed windings for the asymmetrical six-phase IM powered by a two-level VSI connected to a direct current voltage source ($V_{dc}$). In this configuration, each phase of the power converter, composed of two isolated gate bipolar transistors (IGBTs), can be represented by the variable $S$, where $S=1$ indicates the upper IGBT is conducting. At the same time, the lower one is non-conducting, and $S=0$ indicates the opposite state. Consequently, the switching states of the two-level VSI per phase can be organized into a vector, $S=[S_a, S_d, S_b, S_e, S_c, S_f]$, resulting in a total of 64 possible switching combinations corresponding to the number of IM phases. By utilizing $V_{dc}$ and the $S$ vector, the stator phase

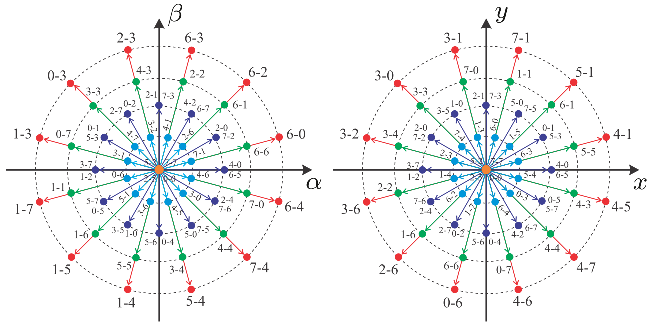


**FIGURE 1.** Voltage vectors of the six-phase IM in the $(\alpha-\beta)$ and $(x-y)$ planes.

voltages can be computed as follows:

$$\begin{bmatrix} v_{as} \\ v_{ds} \\ v_{bs} \\ v_{es} \\ v_{cs} \\ v_{fs} \end{bmatrix} = \underbrace{\frac{V_{dc}}{3}\begin{bmatrix} 2 & 0 & -1 & 0 & -1 & 0 \\ 0 & 2 & 0 & -1 & 0 & -1 \\ -1 & 0 & 2 & 0 & -1 & 0 \\ 0 & -1 & 0 & 2 & 0 & -1 \\ -1 & 0 & -1 & 0 & 2 & 0 \\ 0 & -1 & 0 & -1 & 0 & 2 \end{bmatrix} S^T}_{\text{VSI model}}. \quad (1)$$

Subsequently, to simplify system modelling, the vector space decomposition (VSD) theory based on an invariant amplitude was employed [8]. The stator phase voltages initially expressed in phase variables, as given in (1), are projected into three two-dimensional orthogonal planes $(\alpha-\beta)$, $(x-y)$, and $(z_1-z_2)$ using the transformation matrix $T$ given by (2). This transformation guarantees complete decoupling among the produced planes, attributing electromechanical energy conversion (flux and torque production) to the $(\alpha-\beta)$ plane, while system losses are mapped to the $(x-y)$ plane. The $(z_1-z_2)$ components are disregarded due to the isolated neutral points design of the six-phase IM. Therefore, the resultant voltage vectors can be represented as shown in Fig. 1.

$$T=\frac{1}{3}\begin{bmatrix} 1 & \frac{\sqrt{3}}{2} & -\frac{1}{2} & -\frac{\sqrt{3}}{2} & -\frac{1}{2} & 0 \\ 0 & \frac{1}{2} & \frac{\sqrt{3}}{2} & \frac{1}{2} & -\frac{\sqrt{3}}{2} & -1 \\ 1 & -\frac{\sqrt{3}}{2} & -\frac{1}{2} & \frac{\sqrt{3}}{2} & -\frac{1}{2} & 0 \\ 0 & \frac{1}{2} & -\frac{\sqrt{3}}{2} & \frac{1}{2} & \frac{\sqrt{3}}{2} & -1 \\ 1 & 0 & 1 & 0 & 1 & 0 \\ 0 & 1 & 0 & 1 & 0 & 1 \end{bmatrix}. \quad (2)$$

Moreover, when constructing the discrete state-space model for the system, the stator current and rotor flux components are chosen as the state variables, as indicated in [14]. Consequently, utilizing the forward Euler discretization method, the following expressions can be obtained (3)–(6):

$$I_{s[k+1]} = \mathbf{M_1} I_{s[k]} + \mathbf{M_2}\boldsymbol{\psi}_{r[k]} + \mathbf{M_3} U_{[k]} \quad (3)$$

$$\boldsymbol{\psi}_{r[k+1]} = \mathbf{M_4}\boldsymbol{\psi}_{r[k]} + \mathbf{M_5} I_{s[k]} \quad (4)$$

$$\boldsymbol{\psi}_{s[k+1]} = \mathbf{M_6} I_{s[k+1]} + \mathbf{M_7}\boldsymbol{\psi}_{r[k+1]} \quad (5)$$

$$T_{e[k+1]} = 3P(\psi_{s\alpha[k+1]}\, i_{s\beta[k+1]} - \psi_{s\beta[k+1]}\, i_{s\alpha[k+1]}) \quad (6)$$

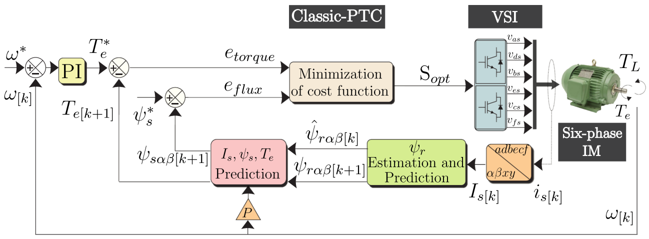


**FIGURE 2.** Classic PTC scheme for a six-phase IM.

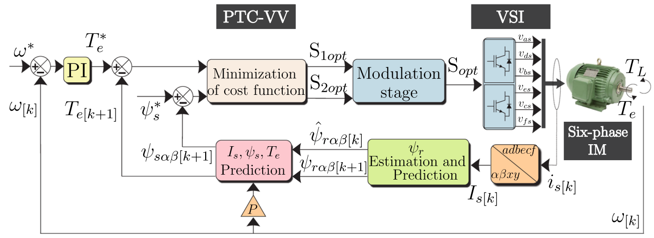


**FIGURE 3.** PTC-VV scheme for a six-phase IM.

being $I_{s[k]} = [i_{s\alpha[k]}, i_{s\beta[k]}, i_{sx[k]}, i_{sy[k]}]$, the stator current vector $\boldsymbol{\psi}_{r[k]} = [\boldsymbol{\psi}_{r\alpha}, \boldsymbol{\psi}_{r\beta}]$, $\boldsymbol{\psi}_{s[k]} = [\boldsymbol{\psi}_{s\alpha}, \boldsymbol{\psi}_{s\beta}, \boldsymbol{\psi}_{sx}, \boldsymbol{\psi}_{sy}]$, the rotor and stator flux vectors, respectively, $T_{e[k+1]}$ the predictive torque and $\mathbf{M_1}$, $\mathbf{M_2}$, $\mathbf{M_3}$, $\mathbf{M_4}$, $\mathbf{M_5}$, $\mathbf{M_6}$, $\mathbf{M_7}$ matrices as described in the Appendix [14].

Where the rotor electrical speed is denoted by $\omega_r = P\omega_m$, $T_s$ represents the sampling period, $M$ represents the mutual inductance, $L_r$ stands for the rotor inductance, $L_s$ stands for the stator inductance, $L_{ls}$ represents the stator leakage inductance, $R_r$ indicates the rotor resistance, $R_s$ indicates the stator resistance of the machine. Also, $\sigma = 1 - M^2/(L_r L_s)$, $\tau_r = L_r/R_r$ and $\tau_s = L_s/R_s$ and $P$ indicates the pole pairs.

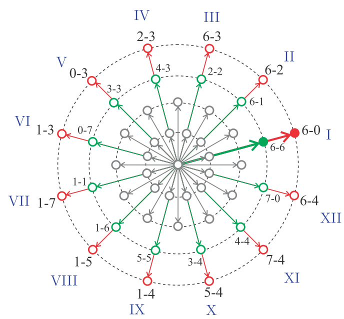


**FIGURE 4.** Virtual voltage vectors for a six-phase IM.

## III. PREDICTIVE TORQUE CONTROLLERS (PTC) FOR SIX-PHASE IM

### A. CLASSIC PTC METHOD

In the classic PTC (Fig. 2), the notation uses a superscript (ˆ) to denote estimation values, while $[k]$ denotes actual samples, and $[k+1]$ denotes predictive values. The external control loop involves a PI controller, which adjusts the mechanical speed and produces the corresponding torque reference $T_e^*$, then compared with its predicted value $T_{e[k+1]}$. Note that $T_{e[k+1]}$ is obtained according to the prediction model, taking into account the estimated and predicted values of the rotor flux, represented as $\hat{\psi}_{r\alpha\beta[k]}$ and $\psi_{r\alpha\beta[k+1]}$, respectively. The stator flux, $\psi_{s\alpha\beta[k+1]}$, is determined using the prediction model and compared with its reference value. The iterative computation of the predictive model incorporates all available voltage vectors defined by the converter model (64 voltage vectors for the adopted converter), along with the measured mechanical speed and stator phase currents. Another crucial consideration is the weighting factors in the cost function (7), which determines the optimal switching state to be applied throughout the entire sampling period in classic PTC for driving the six-phase IM. These weighting factors are essential for properly regulating the $(x-y)$ currents.

$$J = (e_{torque})^2 + K_f(e_{flux})^2 + K_x(e_x)^2 + K_y(e_y)^2 \qquad (7)$$

being $e_{torque} = T_e^* - T_{e[k+1]}$, $e_{flux} = \psi_s^* - \psi_{s[k+1]}$, $e_x = i_{sx}^* - i_{sx}$ and $e_y = i_{sy}^* - i_{sy}$. The $K_f$, $K_x$, and $K_y$ coefficients are the weighting factors for flux and $(x-y)$ currents, respectively, and must be chosen based on the control objective. A significant drawback of the classic PTC strategy is using a single switching state throughout the entire sampling period. This limitation prevents regulating the $(\alpha-\beta)$ and $(x-y)$ planes within the same sampling period, regardless of the weighting factors chosen in the cost function. This issue is addressed in the proposed PTC-VV strategy.

### B. PROPOSED PTC-VV METHOD

This section describes the PTC strategy employing virtual vectors. The diagram in Fig. 3 depicts the block diagram for the PTC-VV approach. One of the primary distinctions between classic PTC and PTC-VV is the number of interactions generated by the predictive model based on the available voltage vectors: 13 voltage vectors for PTC-VV. This reduction in the number of interactions leads to a decrease in computational burden, particularly from the perspective of floating-point operations (FPOs). Through this process, the future values of electrical torque and stator flux are predicted similarly to those in classic PTC. It is important to note that a modulation stage has been incorporated to generate the gating signal for the six-phase IM drive.

Although both classic PTC and PTC-VV strategies share a similar nature, controlling the $(x-y)$ currents present in six-phase IM drives is realized using the concept of virtual vectors. This can be achieved by replacing specific voltage vectors with a new, appropriate combination to ensure minimal or zero average $(x-y)$ voltage production, taking into account the spatial distribution of voltage vectors within the $(\alpha-\beta)$ and $(x-y)$ planes. Using Fig. 4 as a reference, by employing a combination of one medium-large vector (e.g., vector 6-6, green filled circle) and one large voltage vector (e.g., vector 6-0, red filled circle), consisting of 12 pairs of active large and medium voltage vectors, and a single null vector. The selection of these specific vectors is due to the medium-large vector and the large vector having the same direction in the $(\alpha - \beta)$ plane; however, they have opposite directions in the $(x - y)$ plane. This characteristic can help minimize copper losses. The resulting voltage vectors are known as virtual vectors.

To achieve a zero average voltage in the $(x - y)$ plane, it is necessary to apply each pair of voltage vectors at different times during the sampling period. Thus, the duty cycles of the vectors ($d_1$ and $d_2$) are determined through a system of equations that take into account their magnitudes. Consequently, the PTC-VV can be formulated as follows [22]:

$$\mathbf{VV} = d_1 V_{large} + d_2 V_{mid-large} \tag{8}$$

being $d_1 = 0.73\, T_s$ and $d_2 = 0.27\, T_s$.

Afterwards, a new cost function must determine a pair of virtual voltage vectors. Since the algorithm no longer requires the inclusion of secondary components, it becomes feasible to redefine the predictive model. Thus, the cost function of PTC-VV can be expressed as (9), owing to the absence of $(x - y)$ components in the strategy. Subsequently, the selected vectors are forwarded to a modulation stage, where a voltage vector is generated by combining them linearly. Finally, the resultant voltage vector is applied to the two-level VSI, which feeds the six-phase IM.

$$J_1 = (e_{torque})^2 + K_f (e_{flux})^2 \tag{9}$$

being $e_{torque} = T_e^* - T_{e[k+1]}$, $e_{flux} = \psi_s^* - \psi_{s[k+1]}$ and $K_f$ the weighting factor of the flux. It is important to note that fewer terms characterize the cost function. This approach effectively reduces the computational burden of the PTC-VV compared to classic PTC. Fig. 5 presents a straightforward flowchart for implementing the PTC-VV.

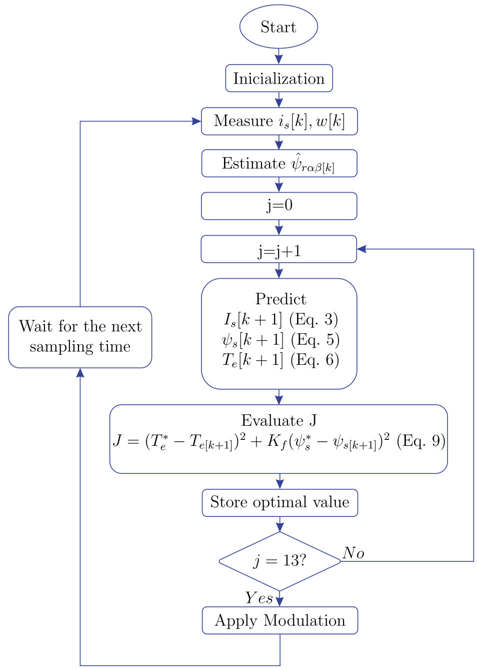


**FIGURE 5.** Flowchart of the execution of the PTC-VV.

**TABLE 1.** Parameters of the Six-Phase IM

| PARAMETER | VALUE | PARAMETER | VALUE |
|---|---|---|---|
| $R_r$ (Ω) | 6.9 | $R_s$ (Ω) | 6.7 |
| $L_s$ (mH) | 654.4 | $L_r$ (mH) | 626.8 |
| $L_m$ (mH) | 614 | $L_{ls}$ (mH) | 5.3 |
| $\omega_{m-rated}$ (r/min) | 2540 | $P_w$ (kW) | 1.5 |
| $J_i$ (kg.m$^2$) | 0.07 | $B_i$ (kg.m$^2$/s) | 0.0004 |
| $P$ | 1 | $T_{e-rated}$ (N.m) | 5.6 |
| $V_s$ (V) | 220 | $f_{rated}$ (Hz) | 50 |
| $i_{s-rms}$ (A) | 2.2 | $V_{dc}$ (V) | 400 |
| Efficiency (%) | 86 | Power Factor | 0.8 |

## IV. EXPERIMENTAL RESULTS

This section evaluates how PTC-VV performs during transient and steady-state operations and compares its performance with that of classic PTC through experimental results.

### A. TEST BENCH

The performance of algorithms is assessed using an experimental test setup comprising a six-phase IM, two conventional three-leg VSIs, and a dc power source. Control of the VSIs is achieved using a dSPACE MABXII real-time rapid prototyping platform programmed with MATLAB/Simulink. The parameters of the six-phase IM were determined through standstill tests and conventional AC time-domain methods. These parameters are detailed in Table 1.

Current measurements were taken using LA 55-P sensors with multiple turns for improved accuracy, especially in low measurements. They operate within a frequency range from dc up to 200 kHz and are digitized using a 16-bit A/D converter. The mechanical angle of the six-phase IM is obtained using a 1024 ppr incremental encoder, which allows for the calculation of rotor speed. A variable mechanical load is applied to the six-phase IM using a 5 HP eddy current brake. Finally, the experimental test bench is shown in Fig. 6.

### B. FIGURES OF MERIT

Experimental results demonstrate the effectiveness of the controller through the MSE between the reference and measured variables, including torque, flux, and $(x - y)$ currents. The MSE is defined as $\text{MSE}_m = \sqrt{\frac{1}{N}\sum_{k=1}^{N}(m_{[k]} - m^*_{[k]})^2}$, where $N$ represents the number of samples, $m^*_{[k]}$ denotes the reference variables, $m_{[k]}$ stands for the measured variables, and $m \in T_e, \psi_s, x, y$. Furthermore, $\text{MSE}_{xy}$ is defined as the average value of $\text{MSE}_x$ and $\text{MSE}_y$.

Additionally, the THD of the stator current is computed to comprehensively analyze the system, primarily in terms of the alpha stator current ($\text{THD}_\alpha$), but also in terms of the a-phase stator current ($\text{THD}_\text{a}$), which includes all harmonic

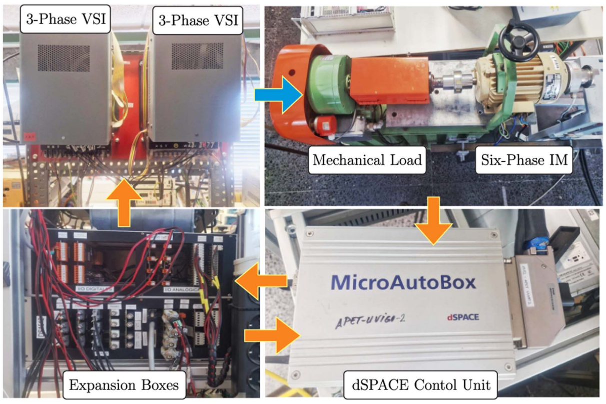


**FIGURE 6.** Experimental test bench including the six-phase IM, the dSPACE platform, the eddy current brake and the two-level VSI.

currents from both $(\alpha - \beta)$ and $(x - y)$ planes. The THD is defined as $\mathrm{THD}_n = \sqrt{\frac{1}{i_{sn1}^2}\sum_{j=2}^{N}(i_{snj})^2}$, where $n \in$ a, $\alpha$. Here, $i_{sn1}$ denotes the fundamental component of the stator current, and $i_{snj}$ represents the harmonic stator current order.

### C. STEADY-STATE OPERATION

Experimental validations have demonstrated the effectiveness of both classic PTC and PTC-VV strategies.

First, a weighting factor for classic PTC must be adjusted to evaluate the performance of both strategies. This adjustment process has been accomplished using a heuristic method to ensure suitable operation under various conditions while considering the tracking of the reference variables under analysis. Different weighing factors were experimented for flux ($K_f$) and $(x - y)$ currents ($K_x$, $K_y$). It was observed that when the weighting factors for $K_f$, $K_x$, and $K_y$ are tuned to high values, the torque is affected. Conversely, when they are set to low values, the $(x - y)$ currents become higher and affect the system's behaviour. Consequently, the tuning resulting in desirable $(x - y)$ currents and reduced torque ripple was $K_f = 10$, $K_x = K_y = 0.2$.

For the analysis, both classic PTC and PTC-VV are investigated under steady-state conditions at different operating points. The sampling frequency is set to 22 kHz. The $(x - y)$ current references are set to zero ($i_{sx}^* = i_{sy}^* = 0$) for the classic PTC because this plane is explicitly associated with losses in the six-phase IM. For this test, two cases were carried out: load variation at a fixed speed and speed variation at a fixed load.

A variation in load torque from 10% to 50% of nominal torque is applied at a constant speed of 1000 r/min, using a 5 HP eddy current brake. A load torque of 80% of nominal torque is also considered at 1500 r/min. The steady-state response of both strategies is listed in Table 2. It can be noted that the PTC-VV has notably good performance at all points of operation, presenting lower $\mathrm{MSE}_x$ and $\mathrm{MSE}_y$ values, compared to the classic PTC. Regarding $\mathrm{MSE}_{Te}$, the PTC-VV

**TABLE 2.** Steady-State Performance Analysis of the PTC Methods Under Different Loads

| $T_L$ (N.m) at $\omega_m^*$ (r/min) | Method | $\mathrm{MSE}_{Te}$ (N.m) | $\mathrm{MSE}_{\psi_s}$ (Wb) | $\mathrm{MSE}_x$ (A) | $\mathrm{MSE}_y$ (A) | $\mathrm{THD}_\alpha$ (%) |
|---|---|---|---|---|---|---|
| 0.1 $T_{nom}$ at 1000 | Classic PTC | 0.5373 | 0.0055 | 1.5293 | 1.5247 | 29.53 |
| | PTC-VV | 0.3286 | 0.0057 | 0.1873 | 0.1799 | 20.41 |
| 0.2 $T_{nom}$ at 1000 | Classic PTC | 0.4819 | 0.0057 | 1.4936 | 1.4966 | 26.56 |
| | PTC-VV | 0.3380 | 0.0059 | 0.1832 | 0.1846 | 17.17 |
| 0.3 $T_{nom}$ at 1000 | Classic PTC | 0.4594 | 0.0057 | 1.5136 | 1.4704 | 23.80 |
| | PTC-VV | 0.3083 | 0.0059 | 0.1881 | 0.1881 | 16.29 |
| 0.4 $T_{nom}$ at 1000 | Classic PTC | 0.4916 | 0.0053 | 1.4520 | 1.4791 | 20.70 |
| | PTC-VV | 0.3094 | 0.0054 | 0.2029 | 0.2162 | 11.44 |
| 0.5 $T_{nom}$ at 1000 | Classic PTC | 0.4994 | 0.0053 | 1.5324 | 1.4655 | 17.86 |
| | PTC-VV | 0.3413 | 0.0052 | 0.2175 | 0.2250 | 10.50 |
| 0.8 $T_{nom}$ at 1500 | Classic PTC | 0.6209 | 0.0068 | 1.4470 | 1.5783 | 14.20 |
| | PTC-VV | 0.5871 | 0.0050 | 0.3059 | 0.2999 | 10.42 |

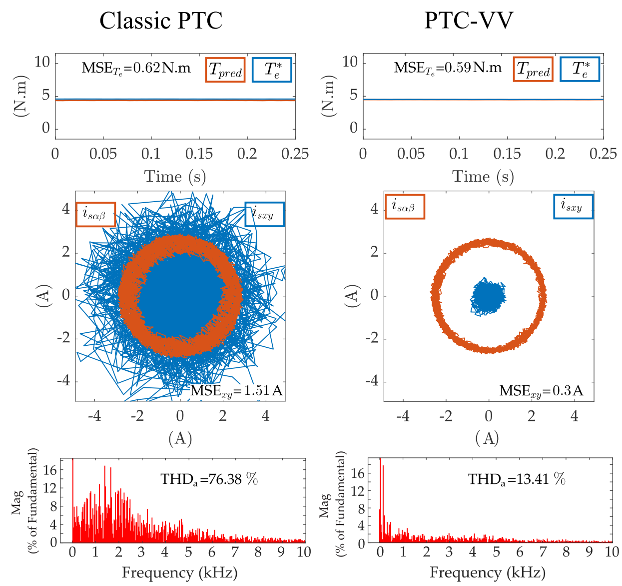


**FIGURE 7.** Steady-state analysis at 80% of nominal torque running at 1500 r/min: From top to bottom for both classic PTC (left column) and PTC-VV (right column): Torque; stator currents in $(\alpha - \beta)$ and $(x - y)$ planes; and harmonic spectrum of the a-phase stator current.

performs better than the classic PTC. However, both strategies have very close values concerning $\mathrm{MSE}_{\psi_s}$. Additionally, the THD for both methods has been taken into consideration. In this context, the PTC-VV has reduced its $\mathrm{THD}_\alpha$ in 41.2%, operating at 50% of nominal torque. Regarding the last row of Table 2, the following reductions have been recorded for PTC-VV compared to the classic PTC: 5.4% in $\mathrm{MSE}_{Te}$, 80% in $\mathrm{MSE}_{xy}$, and 26.6% in $\mathrm{THD}_\alpha$, respectively. It is important to highlight the substantial reduction in the $(x - y)$ currents achieved with PTC-VV, indicating that this strategy effectively reduces copper losses, which is one of the aims of this work. Moreover, Fig. 7 has been included, depicting the performance of both strategies at 80% of nominal torque running at 1500 r/min. The figure shows, from top to bottom, the waveforms for both classic PTC (left column) and PTC-VV

**TABLE 3. Steady-State Performance Analysis of the PTC Methods Under Different Speeds**

| $\omega_m^*$ (r/min) at $T_L$ (N.m) | Method | $\text{MSE}_{Te}$ (N.m) | $\text{MSE}_{\psi_s}$ (Wb) | $\text{MSE}_x$ (A) | $\text{MSE}_y$ (A) | $\text{THD}_\alpha$ (%) |
|---|---|---|---|---|---|---|
| 500 at 0.25 $T_{nom}$ | Classic PTC | 0.3398 | 0.0052 | 1.3701 | 1.3225 | 21.93 |
| | PTC-VV | 0.1829 | 0.0054 | 0.1807 | 0.1726 | 12.54 |
| 1000 at 0.25 $T_{nom}$ | Classic PTC | 0.4833 | 0.0054 | 1.5279 | 1.5070 | 25.14 |
| | PTC-VV | 0.3025 | 0.0056 | 0.1831 | 0.1896 | 14.55 |
| 1500 at 0.25 $T_{nom}$ | Classic PTC | 0.6543 | 0.0057 | 1.5010 | 1.4739 | 25.29 |
| | PTC-VV | 0.5347 | 0.0070 | 0.1856 | 0.1904 | 21.22 |
| 1500 at 0.80 $T_{nom}$ | Classic PTC | 0.6209 | 0.0068 | 1.4470 | 1.5783 | 14.20 |
| | PTC-VV | 0.5871 | 0.0050 | 0.3059 | 0.2999 | 10.42 |

**TABLE 4. Performance Analysis of the PTC-VV Method Under Low Speed Operation**

| $\omega_m^*$ (r/min) at $T_L$ (N.m) | $\text{MSE}_{Te}$ (N.m) | $\text{MSE}_{\psi_s}$ (Wb) | $\text{MSE}_x$ (A) | $\text{MSE}_y$ (A) | $\text{THD}_\alpha$ (%) |
|---|---|---|---|---|---|
| 50 at 0.10 $T_{nom}$ | 0.2132 | 0.0052 | 0.1645 | 0.1769 | 16.09 |
| 100 at 0.20 $T_{nom}$ | 0.2700 | 0.0051 | 0.2248 | 0.1725 | 14.12 |
| 250 at 0.50 $T_{nom}$ | 0.6146 | 0.0045 | 0.2018 | 0.1741 | 21.29 |

(right column), including torque, stator currents in the $(\alpha - \beta)$ and $(x - y)$ planes, and $\text{THD}_\text{a}$, which shows a reduction of 82.4% for PTC-VV compared to classic PTC. These results confirm the superior performance of PTC-VV in improving current quality and reducing harmonic distortion.

Furthermore, the PTC algorithms are tested at steady-state operation by varying the speed reference from 500 r/min to 1500 r/min on the six-phase IM drive system at 25% of nominal torque for both strategies. A speed reference of 1500 r/min at 80% of nominal torque has also been tested. The results are recorded in Table 3. The $\text{THD}_\alpha$ for the PTC-VV is reduced in 33.2% on average compared to the classic PTC. It is clear that the PTC-VV also drastically reduces the content of $(x - y)$ current harmonics due to the application of virtual vectors. Additionally, the $\text{MSE}_{Te}$ is reduced in 31% on average compared to the classic PTC. It is noteworthy that the PTC-VV strategy has also been tested under low-speed operation with load conditions, as presented in Table 4. The performance metrics indicate that PTC-VV performs well, particularly in terms of $\text{MSE}_x$, $\text{MSE}_y$ and $\text{THD}_\alpha$.

### *D. DYNAMIC RESPONSE OF PTC STRATEGIES*

#### 1) SPEED RESPONSE

The experimental study compares the dynamic response of classic PTC and PTC-VV strategies. Both strategies utilize the same outer PI speed controller. In that sense, while the six-phase IM is running at 1000 r/min, a reversing test is conducted by altering the command speed from 1000 r/min to −1000 r/min at a load of 10% of nominal torque. The maximum torque is limited during the transient to a value of approximately $\sqrt{2} \times T_\text{nom}$. The drive's response for both strategies is depicted in Fig. 8. The stator flux is maintained at its nominal value. This test investigates the performance of

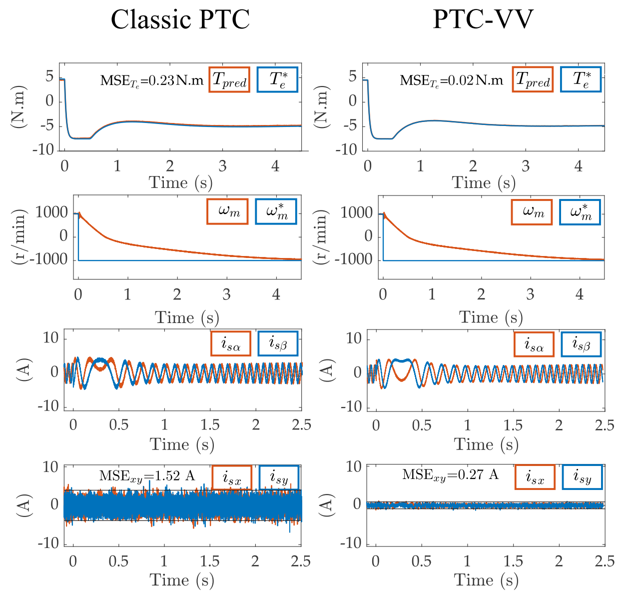


**FIGURE 8. Dynamic response analysis from 1000 r/min to −1000 r/min (transient condition): From top to bottom for both classic PTC (left column) and PTC-VV (right column): Torque; rotor mechanical speed; stator current in $(\alpha - \beta)$ plane; and stator current in $(x - y)$ plane.**

both algorithms at different operating points. Notably, from 1000 r/min to −1000 r/min, it can be observed that both strategies exhibit similar transient responses in terms of overshoot and reaching time of 0.5 ms. It is also noted that both strategies can successfully track their references, highlighting that the PTC-VV shows better performance compared to the classic PTC, in terms of $\text{MSE}_{Te}$ leading to a 91% reduction. Fig. 8 also shows the rotor mechanical speed and the stator currents in the $(\alpha - \beta)$ and $(x - y)$ planes, from top to bottom, respectively, for both strategies. The stator current waveform in the $(\alpha - \beta)$ plane remains sinusoidal throughout the operation. However, a notable enhancement in the $(x - y)$ currents can be observed for the PTC-VV strategy compared to the classic PTC, as evidenced by $\text{MSE}_{xy}$, resulting in an 82% reduction over the classic PTC. This improvement in the $(x - y)$ currents is due to the application of virtual vectors, which nullifies the $(x - y)$ voltage vectors.

#### 2) TORQUE RESPONSE

The transient response of PTC algorithms is evaluated using a six-phase IM drive setup under varying load torque conditions, and waveforms are acquired. A load torque equal to 80% of the nominal torque is applied to the six-phase IM running at a constant speed of 1500 r/min. The response of both strategies is shown in Fig. 9. The torque achieves its desired value within 50 ms for both methods. The rotor speed undergoes a transient drop due to the applied load and subsequently returns to a steady-state in both cases. From top to bottom, the figure presents the waveforms for Classic PTC (left column) and PTC-VV (right column), including torque, rotor speed, and stator currents in the $(\alpha - \beta)$ and $(x - y)$

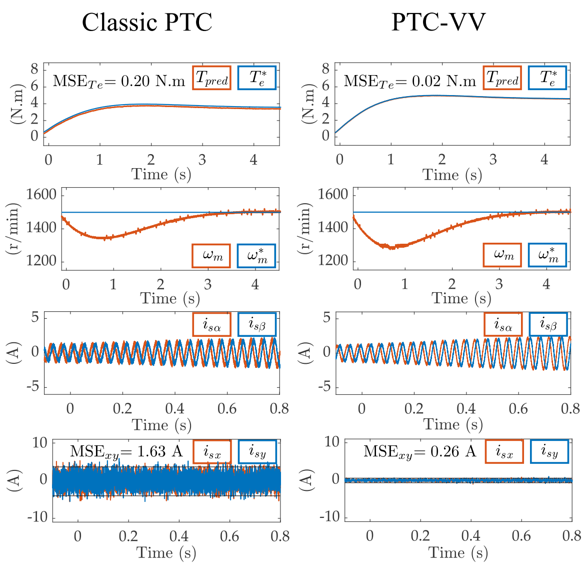


**FIGURE 9.** Comparative response to step load torque at 1500 r/min: From top to bottom for both classic PTC (left column) and PTC-VV (right column): Torque; rotor speed; stator current ($\alpha-\beta$) plane; and stator current ($x-y$) plane.

planes. Notably, PTC-VV significantly reduces ($x-y$) currents, effectively minimizing copper losses, a key objective of this work.

### 3) COMPUTATIONAL BURDEN

The comparative analysis also examined the computational burden. The number of FPOs was considered a critical parameter in this regard. As highlighted in the recent survey on fast FCS-MPC methods for multiphase drives [36], reducing execution time and computational complexity is key to enabling real-time implementation. The voltage vectors used in the PTC strategies (classic PTC, SMPTC, PTC-VV) were considered, representing the number of iterations carried out in every sampling period involved in prediction computation, cost function minimization, and the modulation process. A quantitative analysis of the computational burden has been incorporated, comparing the proposed PTC-VV method with the classic PTC and the recent SMPTC strategy. Classic PTC requires 3968 FPOs per sampling period. SMPTC reduces this to 1958 FPOs, while the proposed PTC-VV further lowers it to 806 FPOs by synthesizing only 13 virtual vectors and simplifying the cost function. This represents a 79.7% reduction compared to classic PTC and 58.8% compared to SMPTC. The detailed comparison is summarized in Table 5.

Additionally, the execution time of each control algorithm was experimentally measured using the dSPACE MABXII platform. The proposed PTC-VV strategy achieves a computational time of 8.4 $\mu$s, which represents a 49.7% reduction compared to the classic PTC (16.7 $\mu$s) and a 32.8% reduction compared to the SMPTC (12.5 $\mu$s). These results confirm the significant computational efficiency of the PTC-VV method, making it a suitable solution for real-time industrial control applications.

**TABLE 5.** Computational Burden Comparison

| Control Strategy | Vectors Evaluated | Structure | FPOs per Sample | Computational Burden ($\mu$s) |
|---|---|---|---|---|
| Classic PTC | 49 (all) | Single-stage | 3968 | 16.7 |
| SMPTC | 13 | Three-stage (sequential) | 1958 | 12.5 |
| Proposed PTC-VV | 13 (VV) | Single-stage (reduced cost function) | 806 | 8.4 |

**TABLE 6.** Experimental Comparison at the Same Average Switching Frequency About of 3.6 kHz

| $\omega_m^*$ (r/min) | Method | MSE$_x$ (A) | MSE$_y$ (A) | THD$_\alpha$ (%) | THD$_a$ (%) | $f_s$ (kHz) | $f_{sw}$ (kHz) |
|---|---|---|---|---|---|---|---|
| 500 | Classic PTC | 1.3718 | 1.3896 | 15.85 | 82.15 | 22 | 3.9 |
| | PTC-VV | 0.1614 | 0.1396 | 15.34 | 17.19 | 8 | 3.7 |
| 1000 | Classic PTC | 1.4839 | 1.5057 | 14.27 | 77.83 | 22 | 3.6 |
| | PTC-VV | 0.1845 | 0.1670 | 12.42 | 12.38 | 8 | 3.4 |
| 1500 | Classic PTC | 1.3890 | 1.4834 | 13.74 | 72.14 | 22 | 3.6 |
| | PTC-VV | 0.1865 | 0.1817 | 12.63 | 12.65 | 8 | 3.2 |

### 4) EVALUATION AT THE SAME SWITCHING FREQUENCY

For a fair comparison, the same average switching frequency should be considered. To achieve this, the sampling frequency ($f_s$) of the PTC-VV strategy is reduced to 8kHz, resulting in an average switching frequency ($f_{sw}$) of 3.6kHz, as the PTC-VV utilizes a two-vector scheme. The tests for both PTC controllers were conducted at varying speeds under the same load conditions. Notably, in terms of MSE$_x$, MSE$_y$, and MSE$_{Te}$, the PTC-VV demonstrates superior performance compared to the classic PTC, as shown in Table 6. Also, the proposed strategy presents better performance compared to SMPTC, which was tested at a 20 kHz sampling frequency, requiring a higher sampling rate and thereby increasing the computational burden [34]. Regarding the THD$_\alpha$, PTC controllers exhibit similar performance. However, the PTC-VV significantly reduces the THD$_a$ compared to the classic PTC, leading to a 95.2% reduction in copper losses or approximately 40 W, considering all harmonic currents, this power value was obtained considering the rms value of the phase currents with classic PTC and PTC-VV, and applying the $i_s^2 R_s$ equation. Considering an approximate electrical power of 1 kW, a 4% improvement in efficiency, compared to classic PTC, is observed.

## *E. CONTROL SENSITIVITY TO PARAMETERS MISMATCH*

The robustness study involves comparing the performance of PTC-VV at the nominal value of $L_m$, with a variation of $\pm$ 25%, as $L_m$ is considered the most sensitive parameter in six-phase IM [37]. This variation accounts for the effect of magnetic saturation, which typically causes the $L_m$ value to

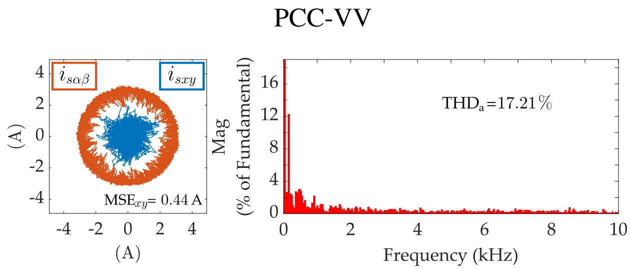


**FIGURE 10.** Steady-state performance of the PCC-VV strategy at 1500 r/min and 80% of nominal torque. Stator currents in the $(\alpha - \beta)$ and $(x - y)$ planes (left column), and harmonic spectrum of the a-phase stator current (right column).

fluctuate within this range. For this purpose, the magnetizing inductance value is modified in the implemented control block, thereby emulating an error in the measurement of $L_m$. Notably, a decrease in magnetizing inductance is observed as the torque increases, a trend consistent with the findings reported in [37]. Although multiple results were obtained for different mismatch scenarios, only one representative case is presented here, as the others demonstrated similar dynamic behavior. The results at 1500 r/min under a load torque equal to 80% of the nominal torque, demonstrate that PTC-VV exhibits significant robustness, showing minimal changes in performance compared to the nominal $L_m$. Specifically, PTC-VV achieves notable results, computing 0.2782 A for MSE$_x$, 0.2735 A for MSE$_y$ and 12.29% for THD$_\alpha$. Furthermore, PTC-VV shows no overshoot and achieves a settling time of 0.5 ms.

### F. EXPERIMENTAL EVALUATION OF PREDICTIVE CURRENT CONTROL WITH VIRTUAL VECTORS

In order to establish a benchmark for control strategies based on virtual voltage vectors in six-phase IMs, an experimental evaluation of the predictive current control method using virtual vectors (PCC-VV) was performed. The test was conducted under steady-state conditions at 1500 r/min with a load torque of 80% of the nominal value, using the same hardware platform and measurement setup employed in the previous PTC experiments (Fig. 7). This ensures a consistent and meaningful comparison framework. The results, illustrated in Fig. 10, demonstrate that the proposed PTC-VV strategy achieves superior current quality and improved harmonic suppression compared to PCC-VV under identical operating conditions, particularly in terms of $(x - y)$ current regulation. These findings further validate the enhanced performance of PTC-VV when employing virtual voltage vectors in predictive control.

## V. CONCLUSION

This paper introduces a PTC scheme designed for a six-phase IM using a virtual vector strategy. Compared to classic PTC, this strategy reduces stator $(x - y)$ currents, which in turn mitigates copper losses. A significant advantage of PTC-VV is its ability to reduce the computational burden by limiting the total number of voltage vectors to 13 virtual voltage vectors. The presented results, under both transient and steady-state conditions, demonstrate that PTC-VV effectively reduces currents in the secondary plane while maintaining torque and flux control tracking. Also, it is important to highlight the performance of the PTC-VV in terms of THD, showing that the PTC-VV maintains a lower value compared to the classic PTC under torque and speed response. At the same time, PTC-VV shows a significant improvement in computational burden and an improvement in energy efficiency considering the substantial reduction of harmonic currents, especially in the $(x - y)$ plane. By improving current regulation and mitigating conduction losses, the proposed PTC-VV strategy demonstrates enhanced performance and achieves a computational time of 8.4 $\mu$s, resulting in a 49.7% and 32.8% reduction compared to the classic PTC and SMPTC, respectively. These improvements validate the proposed method as a competitive and efficient alternative for real-time control in multiphase drive systems. Furthermore, the experimental comparison with the PCC-VV strategy was carried out to assess the performance of PTC-VV in terms of $(x - y)$ current regulation and harmonic distortion reduction, further validating the proposed PTC-VV method for practical use in predictive control applications.

## APPENDIX

$$\mathbf{M_1} = \mathrm{diag}\left[A_{11}\ A_{22}\ A_{33}\ A_{44}\right]$$

$$A_{11} = A_{22} = 1 - \frac{T_s}{\sigma\tau_s} - \frac{(1-\sigma)T_s}{\sigma\tau_r}$$

$$A_{33} = A_{44} = 1 - \frac{R_s T_s}{L_{ls}}$$

$$\mathbf{M_2} = \begin{bmatrix} \frac{R_r M T_s}{\sigma L_s L_r^2} & \frac{\omega_r M T_s}{\sigma L_s L_r} \\ -\frac{\omega_r M T_s}{\sigma L_s L_r} & \frac{R_r M T_s}{\sigma L_s L_r^2} \\ 0 & 0 \\ 0 & 0 \end{bmatrix}$$

$$\mathbf{M_3} = \mathrm{diag}\left[\frac{T_s}{\sigma L_s}\ \frac{T_s}{\sigma L_s}\ \frac{T_s}{\sigma L_s}\ \frac{T_s}{\sigma L_s}\right]$$

$$\mathbf{M_4} = \begin{bmatrix} 1 - \frac{T_s}{\tau_r} & -\omega_r T_s \\ \omega_r T_s & 1 - \frac{T_s}{\tau_r} \end{bmatrix}, \mathbf{M_5} = \begin{bmatrix} \frac{M T_s}{\tau_r} & 0 & 0 & 0 \\ 0 & \frac{M T_s}{\tau_r} & 0 & 0 \end{bmatrix}$$

$$\mathbf{M_6} = \mathrm{diag}\left[\sigma L_s\ \sigma L_s\ L_{ls}\ L_{ls}\right], \mathbf{M_7} = \begin{bmatrix} \frac{M}{L_r} & 0 \\ 0 & \frac{M}{L_r} \\ 0 & 0 \\ 0 & 0 \end{bmatrix}$$

## REFERENCES

[1] A. G. Yepes et al., “A comprehensive survey on fault tolerance in multiphase AC drives, Part 1: General overview considering multiple fault types,” *Machines*, vol. 10, no. 3, 2022, Art. no. 208.

[2] E. Prieto-Araujo, A. Junyent-Ferré, D. Lavèrnia-Ferrer, and O. Gomis-Bellmunt, "Decentralized control of a nine-phase permanent magnet generator for offshore wind turbines," *IEEE Trans. Energy Conver.*, vol. 30, no. 3, pp. 1103–1112, Sep. 2015.

[3] "TM4 Dana," (n.d.). Accessed: Apr. 11, 2025. [Online]. Available: https://www.audi-mediacenter.com/en/press-releases/audi-presents-e-tron-fe07-for-formula-e-world-championship-13365

[4] "E-tron FE07," (n.d.). Accessed: Apr. 11, 2025. [Online]. Available: https://www.audi-mediacenter.com/en/press-releases/audi-presents-e-tron-fe07-for-formula-e-world-championship-13365

[5] "BMW iX M60," (n.d.). Accessed: Apr. 11, 2025. [Online]. Available: https://www.carscoops.com/2022/01/bmw-ix-m60-the-performance-flagship-of-the-electric/

[6] M. A. Frikha, J. Croonen, K. Deepak, Y. Benômar, M. El Baghdadi, and O. Hegazy, "Multiphase motors and drive systems for electric vehicle powertrains: State of the art analysis and future trends," *Energies*, vol. 16, no. 2, 2023, Art. no. 768.

[7] F. Barrero and M. J. Duran, "Recent advances in the design, modeling, and control of multiphase machines-Part I," *IEEE Trans. Ind. Electron.*, vol. 63, no. 1, pp. 449–458, Jan. 2016.

[8] Y. Zhao and T. A. Lipo, "Space vector PWM control of dual three-phase induction machine using vector space decomposition," *IEEE Trans. Ind. Appl.*, vol. 31, no. 5, pp. 1100–1109, Sep./Oct. 1995.

[9] R. Bojoi, F. Farina, F. Profumo, and A. Tenconi, "Dual-three phase induction machine drives control-A survey," *IEEJ Trans. Industry Appl.*, vol. 126, no. 4, pp. 420–429, 2006.

[10] G. K. Singh, K. Nam, and S. K. Lim, "A simple indirect field-oriented control scheme for multiphase induction machine," *IEEE Trans. Ind. Electron.*, vol. 52, no. 4, pp. 1177–1184, Aug. 2005.

[11] J. K. Pandit, M. V. Aware, R. V. Nemade, and E. Levi, "Direct torque control scheme for a six-phase induction motor with reduced torque ripple," *IEEE Trans. Power Electron.*, vol. 32, no. 9, pp. 7118–7129, Sep. 2017.

[12] Y. Zhang, J. Zhu, Z. Zhao, W. Xu, and D. G. Dorrell, "An improved direct torque control for three-level inverter-fed induction motor sensorless drive," *IEEE Trans. Power Electron.*, vol. 27, no. 3, pp. 1502–1513, Mar. 2012.

[13] J. Beerten, J. Verveckken, and J. Driesen, "Predictive direct torque control for flux and torque ripple reduction," *IEEE Trans. Ind. Electron.*, vol. 57, no. 1, pp. 404–412, Jan. 2010.

[14] P. Gonçalves, S. Cruz, and A. Mendes, "Finite control set model predictive control of six-phase asymmetrical machines-An overview," *Energies*, vol. 12, no. 24, 2019, Art. no. 4693.

[15] M. Ayala, J. Doval-Gandoy, J. Rodas, O. Gonzalez, R. Gregor, and M. Rivera, "A novel modulated model predictive control applied to six-phase induction motor drives," *IEEE Trans. Ind. Electron.*, vol. 68, no. 5, pp. 3672–3682, May 2021.

[16] C. S. Lim, E. Levi, M. Jones, N. A. Rahim, and W. P. Hew, "FCS-MPC-Based current control of a five-phase induction motor and its comparison with PI-PWM control," *IEEE Trans. Ind. Electron.*, vol. 61, no. 1, pp. 149–163, Jan. 2014.

[17] C. Zhang, C. Liu, and X. Xing, "An optimized model predictive control method with fixed switching frequency for eliminating common-mode voltage of five-level converters," *IEEE Trans. Ind. Inform.*, vol. 20, no. 2, pp. 1432–1444, Feb. 2024.

[18] J. Rodriguez et al., "Latest advances of model predictive control in electrical drives—Part II: Applications and benchmarking with classical control methods," *IEEE Trans. Power Electron.*, vol. 37, no. 5, pp. 5047–5061, May 2022.

[19] D. Schuetz et al., "Space vector modulated model predictive control for grid-tied converters," *IEEE Trans. Ind. Inform.*, vol. 19, no. 1, pp. 414–425, Jan. 2023.

[20] S. Vazquez, J. Rodriguez, M. Rivera, L. G. Franquelo, and M. Norambuena, "Model predictive control for power converters and drives: Advances and trends," *IEEE Trans. Ind. Electron.*, vol. 64, no. 2, pp. 935–947, Feb. 2017.

[21] L. Zheng, J. E. Fletcher, B. W. Williams, and X. He, "A novel direct torque control scheme for a sensorless five-phase induction motor drive," *IEEE Trans. Ind. Electron.*, vol. 58, no. 2, pp. 503–513, Feb. 2011.

[22] I. Gonzalez-Prieto, M. J. Duran, J. J. Aciego, C. Martin, and F. Barrero, "Model predictive control of six-phase induction motor drives using virtual voltage vectors," *IEEE Trans. Ind. Electron.*, vol. 65, no. 1, pp. 27–37, Jan. 2018.

[23] O. Gonzalez et al., "Model predictive current control of six-phase induction motor drives using virtual vectors and space vector modulation," *IEEE Trans. Power Electron.*, vol. 37, no. 7, pp. 7617–7628, Jul. 2022.

[24] Y. Zhang and H. Yang, "Two-vector-based model predictive torque control without weighting factors for induction motor drives," *IEEE Trans. Power Electron.*, vol. 31, no. 2, pp. 1381–1390, Feb. 2016.

[25] T. Geyer, G. Papafotiou, and M. Morari, "Model predictive direct torque control—Part I: Concept, algorithm, and analysis," *IEEE Trans. Ind. Electron.*, vol. 56, no. 6, pp. 1894–1905, Jun. 2009.

[26] J. A. Riveros, F. Barrero, E. Levi, M. J. Durán, S. Toral, and M. Jones, "Variable-speed five-phase induction motor drive based on predictive torque control," *IEEE Trans. Ind. Electron.*, vol. 60, no. 8, pp. 2957–2968, Aug. 2013.

[27] Y. Zhang, H. Yang, and B. Xia, "Model-predictive control of induction motor drives: Torque control versus flux control," *IEEE Trans. Ind. Appl.*, vol. 52, no. 5, pp. 4050–4060, Sep./Oct. 2016.

[28] J. Rodriguez, R. M. Kennel, J. R. Espinoza, M. Trincado, C. A. Silva, and C. A. Rojas, "High-performance control strategies for electrical drives: An experimental assessment," *IEEE Trans. Ind. Electron.*, vol. 59, no. 2, pp. 812–820, Feb. 2012.

[29] E. Maqueda et al., "Speed control of a six-phase IM fed by a multi-modular matrix converter using an inner PTC with reduced computational burden," *IEEE Access*, vol. 9, pp. 160035–160047, 2021.

[30] A. Bhowate, M. V. Aware, and S. Sharma, "Speed sensor-less predictive torque control for five-phase induction motor drive using synthetic voltage vectors," *IEEE J. Emerg. Sel. Topics Power Electron.*, vol. 9, no. 3, pp. 2698–2709, Jun. 2021.

[31] Y. Luo and C. Liu, "A simplified model predictive control for a dual three-phase PMSM with reduced harmonic currents," *IEEE Trans. Ind. Electron.*, vol. 65, no. 11, pp. 9079–9089, Nov. 2018.

[32] F. Wang, S. Li, X. Mei, W. Xie, J. Rodríguez, and R. M. Kennel, "Model-based predictive direct control strategies for electrical drives: An experimental evaluation of PTC and PCC methods," *IEEE Trans. Ind. Inform.*, vol. 11, no. 3, pp. 671–681, Jun. 2015.

[33] Q. Yuan, R. Xiao, J. Wang, K. Xia, and W. Yu, "Double-virtual-vector-Based model predictive torque control for dual three-phase PMSM," *Electronics*, vol. 14, no. 1, 2024, Art. no. 50.

[34] J. Rodas et al., "Sequential model predictive torque control for six-phase machines without weighting factors," *IEEE Open J. Power Electron.*, vol. 6, pp. 802–810, 2025.

[35] O. Gonzalez et al., "Model predictive torque control based on virtual vectors for six-phase induction machines," in *Proc. IEEE Transp. Electrific. Conf. Expo*, 2024, pp. 1–6.

[36] E. Marsal, M. R. Arahal, M. G. Satué, and M. Perales, "Review of fast computation methods for finite-state predictive control of multi-phase drives," *Appl. Sci.*, vol. 14, no. 24, 2024, Art. no. 11774.

[37] J. Nerg, J. Pyrhönen, J. Partanen, and E. Ritchie, "Induction motor magnetizing inductance modelling as a function of torque," in *Proc. Int. Conf. Elect. Mach.*, 2004.


**OSVALDO GONZALEZ** was born in Asunción, Paraguay. He received the B.Eng. degree in electronic engineering from Universidad Nacional de Asunción (UNA), San Lorenzo, Paraguay, in 2014, and the M.Sc. and Ph.D. degrees in power electronics from the Faculty of Engineering, UNA, in 2017 and 2021, respectively. His research focuses on control of multiphase motors. He was the recipient of the Paraguayan National Science Award.

**JESÚS DOVAL-GANDOY** (Member, IEEE) received the M.S. degree in electrical engineering from the Polytechnic University of Madrid, Madrid, Spain, in 1991, and the Ph.D. degree from the University of Vigo, Vigo, Spain, in 1999. He is currently a Professor and Head with Applied Power Electronics Technology Research Group, University of Vigo. His research focuses on AC power conversion.

**MAGNO AYALA** (Member, IEEE) received the B.Eng. degree in electronic engineering from the Universidad Nacional de Asunción (UNA), San Lorenzo, Paraguay, in 2014, and the M.Sc. and Ph.D. degrees in power electronics from the Faculty of Engineering, UNA, in 2017 and 2020, respectively. His research focuses on control of multiphase AC machines. He was the recipient of the 2020 Paraguayan National Science Award and 2020 from the Industrial Electronics Society in 2021.

**JORGE RODAS** (Senior Member, IEEE) born in Asunción, in 1984. He received the B.Eng. degree in electronic engineering from the Universidad Nacional de Asunción, San Lorenzo, Paraguay, in 2009, the M.Sc. degree from the Universidad de Vigo, Vigo, Spain, in 2012, the second M.Sc. degree from Universidad de Sevilla, Seville, Spain, in 2013, the dual Ph.D. degree from the Universidad Nacional de Asunción and from Universidad de Sevilla, in 2016, and the master's degree from National Defence Council, Paraguay, in 2021. He was a Visiting Professor with École de Technologie Supérieure, Montreal, QC, Canada and Polytechnic University of Catalonia, Barcelona, Spain, in 2017 and 2022, respectively. In 2011, he joined Facultad de Ingeniería, Universidad Nacional de Asunción, where he is currently a Professor and Research Director. He has authored and coauthored three book chapters and more than 145 journal and conference papers. His research interests include applications of advanced control to real-world problems, applying finite control set model predictive control and nonlinear control to power electronic converters, renewable energy conversion systems, electric motor drives, and robotic systems (especially unmanned aerial vehicles). Prof. Rodas is also an Associate Editor for Elsevier *Alexandria Engineering Journal* and IEEE Access and Guest Editor of MDPI *World Electric Vehicle Journal*. He was the Guest Editor of IEEE Journal of Emerging and Selected Topics in Power Electronics, MDPI *Energies*, MDPI *Sustainability* and *Frontiers in Energy Research*. He was the recipient of the Paraguayan National Science Award in 2020. He has been categorised at Level III of SISNI. He is also a fellow of the Institute of Engineering and Technology, U.K.

**PAOLA MAIDANA** received the degree in electronic engineering, and the Master of Science degree in power electronics from Facultad de Ingeniería de la Universidad Nacional de Asunción (FIUNA), San Lorenzo, Paraguay. She is currently working toward the Doctoral degree in electronic engineering with Power and Control Systems Laboratory, FIUNA. Her research interests include nonlinear control of electrical drives, multiphase induction machines, and power electronic converters.

**CHRISTIAN MEDINA** received the Master of Science degree in electronic engineering from Facultad de Ingeniería de la Universidad Nacional de Asunción, San Lorenzo, Paraguay, where Christian Medina is currently working toward the Doctoral degree. Christian Medina's research interests include electronic power converters, nonlinear control, and induction machines.

**CARLOS ROMERO** received the bachelor's and master's degrees in electronic engineering from the Faculty of Engineering National University of Asunción (FIUNA), San Lorenzo, Paraguay, in 2014 and 2018, respectively. He has participated in several national and international research projects in the field of electronics. He is currently a Research Professor with the Department of Electronic and Mechatronic Engineering, FIUNA. He is also a Researcher categorized with SISNI, National Council of Science and Technology and Coordinator with the Department of Basic Sciences, FIUNA. His research interests include design and implementation of control strategies in power converter applications, multiphase machines, and printed circuit board designs.

**LARIZZA DELORME** (Member, IEEE) received the B.Eng. degree in electronic engineering from Universidad Nacional de Asunción, San Lorenzo, Paraguay, in 2017, and the M.Sc. degree in electronic engineering, with a focus on renewable energies and energy efficiency from Universidad del Cono Sur de las Américas, Asunción, Paraguay, in 2020. She is currently working toward the Ph.D. degree in power electronics with the Faculty of Engineering, Universidad Nacional de Asunción. Her research interests include modeling, simulation, and advanced control of multiphase electric drive systems.

**RAUL GREGOR** (Member, IEEE) was born in Asunción, Paraguay, in 1979. He received the Engineer degree in electronic engineering from the Catholic University of Asunción, Asunción, in 2005, and the M.Sc. and Ph.D. degrees in electronics, signal processing, and communications from the Higher Technical School of Engineering, University of Seville, Seville, Spain, in 2008 and 2010, respectively. Since 2010, he has been the Head with the Laboratory of Power and Control Systems, Faculty of Engineering National University of Asunción (FIUNA), Asunción. He is currently the Head with the Department of Electronic and Mechatronics Engineering, FIUNA. Since 2017, he has led the technology-based company PQEnerSol SRL, developing cutting-edge technology applied to the energy sector. Dr. Gregor has authored or coauthored about 150 technical papers in the field of power electronics and control systems. His research interests include multiphase drives, advanced control of power converter topologies, power quality, renewable energies, modeling, simulation, optimization, and control of power systems, smart metering and smart grids and predictive control. He was the recipient of the Best Paper Award from the IEEE Transactions on Industrial Electronics, Industrial Electronics Society, in 2010 and Best Paper Award from IET Electric Power Applications, in 2012.

**RICARDO MACIEL** was born in Paraguay, in 1991. He received the bachelor's degree in electrical engineering in 2019 from Universidad Nacional de Asunción, San Lorenzo, Paraguay, where he is currently working toward the M.Sc. degree in power electronics. His research interests include AC power conversion, power system analysis, and renewable energy.